Article

Analysis of Agricultural Drought Evolution Characteristics and Driving Factors in Inner Mongolia Inland River Basin Based on Three-Dimensional Recognition

Zezhong Zhang [1], Hengzhi Guo [1], Kai Feng [1,*], Fei Wang [1], Weijie Zhang [2,3] and Jian Liu [1]

[1] School of Water Conservancy, North China University of Water Resources and Electric Power, Zhengzhou 450046, China; zhangzezhong@ncwu.edu.cn (Z.Z.); ghengzhi@163.com (H.G.); wangfei@ncwu.edu.cn (F.W.); liu_jian1101@163.com (J.L.)

[2] Yinshanbeilu Grassland Eco-Hydrology National Observation and Research Station, China Institute of Water Resources and Hydropower Research, Beijing 100038, China; zhweijie0501@163.com

[3] Institute of Water Resources of Pastoral Area Ministry of Water Resources, Hohhot 010020, China

* Correspondence: fengk0121@163.com; Tel.: +86-1-590-363-8084

Abstract: Agricultural drought events have become more frequent in the Inner Mongolia inland river basin in recent years, and the spatio-temporal evolution characteristics and development rules can be accurately and comprehensively understood using the three-dimensional identification method. In this paper, standardized soil moisture index (SSMI) was used to characterize agricultural drought, and modified Mann–Kendall trend test (MMK) and 3D recognition of drought events were used to analyze the spatio-temporal evolution characteristics of agricultural drought events in this basin and reveal the drought development law. The relationships between drought and temperature (T), precipitation (P), evapotranspiration (E), and humidity (H) were analyzed using a cross-wavelet method. The results are as follows: (1) When the time scale of agricultural drought was short (monthly scale), the alternations of dry and wet were frequent, but the SSMI index of all scales showed a downward trend; (2) The spatial distribution characteristics of drought change trend in four seasons were similar, but the area with a significant downward trend of drought in spring was the largest, and the area of high frequency region was also the largest, and the drought trend was the most obvious; (3) The most serious agricultural drought event occurred from October 2000 to May 2002, and reached its maximum value in September 2001 (drought area and drought severity of 2.26×10^5 km^2 and 3.61×10^5 months·km^2, respectively), which mainly experienced five processes—drought onset–intensification–decay–re-intensification–termination—and the migration path of the drought center showed the characteristics of southwest–northeast transmission; (4) All the four meteorological factors were correlated with SSMI, and P had a greater impact on SSMI. This article aims to reveal the spatio-temporal evolution of agricultural drought events in the Inner Mongolia inland river basin, and provide a new way to accurately evaluate the spatio-temporal evolution of drought.

Keywords: agricultural drought; three-dimensional identification; dynamic evolution; spatio-temporal characteristics; meteorological factors

1. Introduction

Drought is one of the most destructive natural hazards for humans; as the global temperature rises gradually and the shortage of water resources is aggravating, humans face more severe drought situations [1–3]. Once drought occurs, it poses a serious threat to the ecological environment, water resources security, and social economy [4,5]. Drought is a regional phenomenon that changes with time and has significant continuity

and dynamics on the spatio-temporal scale, so it is necessary to accurately and comprehensively understand its spatio-temporal evolution characteristics and development laws [6–8]. Therefore, it is of great significance to accurately evaluate the spatio-temporal dynamic evolution of drought and quantify its characteristics for drought mitigation.

At present, the international classification of drought is generally recognized as meteorological drought, agricultural drought, hydrological drought, or socio-economic drought [9,10]. Agricultural drought refers to the phenomenon of continuous precipitation deficit, resulting in crop reduction or loss of harvest [11,12]. This study of temporal and spatial evolution characteristics of agricultural drought is helpful in analyzing and extracting its law, which has an important role in production and life. Dai et al. analyzed the dynamic evolution characteristics of agricultural drought in the Pearl River Delta by calculating the standardized precipitation index (SPI) [13]. Potopova et al. characterized agricultural drought risk by calculating the standardized precipitation evapotranspiration index (SPEI) of 304 weather stations in the Czech Republic and analyzed the sensitivity of 11 crop yields to SPEI on different time scales during 1951–2012 [14]. Qin et al. compared and analyzed the drought monitoring effect of the Haihe River Basin based on precipitation and soil moisture index from 1960 to 2010 and conducted correlation analysis with normalized difference vegetation index (NDVI), which characterized agricultural drought [15]. The above agricultural drought indicators are analyzed and processed based on the data of ground stations, but the spatial distribution of stations is uneven, and the data of a certain period may be missing, which may deviate from the actual situation. Remote sensing technology has become the most promising technology for drought monitoring due to its advantages of timeliness, efficiency, wide coverage, and data continuity, and it has also achieved good results in practical application [16]. In addition, agricultural drought is mainly due to the decrease in soil water content, which leads to the inability of crops to absorb water from the soil to meet transpiration consumption, thus forming agricultural drought [17]. Relevant studies also show that the water in crops mainly comes from soil water, so the drought index based on soil water content can more truly reflect agricultural drought [18]. Based on the soil water content monitored using remote sensing technology to characterize the standardized soil moisture index (SSMI), it has the advantages of multiple time scales and strong spatio-temporal continuity, which is conducive to the characteristics analysis and rule recognition of drought events. Therefore, SSMI is selected to characterize agricultural drought.

Certain achievements have been made in the study of the spatio-temporal evolution characteristics of drought: Andreadis introduced a clustering algorithm and used the severe-area-duration (S-A-D) curve to analyze the spatial changes in drought events in the United States under a given time [19]. An et al. analyzed the characteristics and changing trend of drought in Inner Mongolia based on the SPEI of different time scales [20]. Zhang et al. analyzed the characteristics of drought in the North China Plain during 1982–2020 using the vegetation health index (VHI) and various climate factors [1]. Du et al. discussed the spatio-temporal evolution of meteorological drought and agricultural drought based on the cultivated land type [21]. In fact, the drought event is an abnormal problem of dry and wet in three dimensions. However, the above research is limited to the analysis of one-dimensional time change trend or two-dimensional spatial change trend, and the dimension reduction in the drought events destroys the three-dimensional spatio-temporal structure of the drought events, which will also lead to the loss of drought characteristic variables [22]. In order to analyze drought events more accurately, scholars have identified and studied drought events based on a three-dimensional perspective. Lloyd-Hughes extended Andreadis' drought identification method, applied the clustering method to three-dimensional space, and made a complete spatio-temporal representation of the drought events [23]. Guo et al. analyzed the drought events by improving the three-dimensional clustering algorithm and extracting multiple feature variables [24]. Wen et al. identified the meteorological drought events in the Huaihe River Basin from 1961 to 2015 via the three-dimensional drought structure and analyzed the spatio-temporal evolution

characteristics of the drought [25]. Feng et al. identified the drought event in the Heihe River Basin during 1961–2018 based on the three-dimensional drought recognition method and extracted several drought characteristic variables such as duration, area, intensity, severity, center, and migration distance [26]. Therefore, it is necessary to analyze drought based on a three-dimensional perspective, which is helpful in extracting multiple drought characteristic variables and accurately revealing the evolution law of drought events.

The Inner Mongolia inland river basin (IMIRB) is the main grain-producing area in China, but because of the vulnerability zone of drought and semi-drought, the economic development process is seriously affected by drought. With the intensification of climate change, agricultural drought events become more frequent in IMIRB, which hinders agricultural development. Studying the agricultural drought in this area is helpful to the development of agriculture, economy, and society. However, previous studies mostly analyzed the spatio-temporal evolution characteristics from a two-dimensional perspective but did not analyze the drought events from a three-dimensional perspective, ignoring the spatio-temporal continuity of drought, resulting in the failure to comprehensively and accurately evaluate the spatio-temporal dynamic evolution of drought [20,27–30]. At the same time, meteorological factors are important driving factors for the occurrence and change in agricultural drought, but the driving mechanism of meteorological factors on agricultural drought in the study area is still unclear. According to the existing studies, the modified Mann–Kendall trend test (MMK) method can be used to analyze the temporal variation trend of drought and further obtain the spatial distribution characteristics of drought variation trend at grid scale so as to analyze the drought variation trend at each grid point. Cross-wavelet transform can be used to reveal the periodicity and correlation of two signals, which is helpful in analyzing the law of change between the two signals.

Therefore, this study uses the MMK trend test, three-dimensional identification method, and cross-wavelet analysis to analyze the spatio-temporal variation characteristics of agricultural drought in this region, reveals the spatio-temporal evolution law of agricultural drought events, and discusses the driving mechanism of meteorological factors on agricultural drought. In view of this, the main research objectives of this paper are as follows: (1) To study the spatio-temporal trends of agricultural drought at different scales from 1960 to 2021; (2) Reveal the spatio-temporal evolution of agricultural drought from a three-dimensional perspective; (3) Clarify the driving mechanism of meteorological factors on agricultural drought. The research results provide a new way to evaluate the spatio-temporal dynamic evolution of drought in this study area.

2. Study Region

The IMIRB is located in the middle of Inner Mongolia. The study area is located at 105°12′~120°70′ E, 40°33′~46°46′ N, bounded by Yanshan Mountain and Helan Mountain in the east and west and Yinshan Mountain and Greater Hinggan Mountains in the north and south. The area is about 316,600 km², with annual average precipitation of 295 mm and average temperatures of 3~7 °C. It consists of a series of grasslands, cultivated land, and sandy land, and the main inland rivers are Tabu River, Uraghel River, Xilin Gol River, Bayin River, and so on. Drought in this region is a serious problem, which easily leads to crop reduction and grassland degradation, which is a great harm to agriculture [31,32]. Therefore, this paper will study the agricultural drought problem in this region, which will help the drought prevention and control in this region in order to reduce the harm caused by drought. The basic situation in the study area map is shown in Figure 1.

Figure 1. Basic situation in the study area. UBB, Urat Rear Banner; UMB, Urat Middle Banner; DM, Darhan Muminggan United Banner; SG, Shiguai District; WC, Wuchuan County; SZW, Siziwang Banner; CRW, Qahar youyi houqi; EL, Erenhot City; SRB, Sonid Right Banner; XB, Xianghuang Banner; SD, Shangdu County; XH, Xilinhot City; SLB, Sonid Left Banner; ZB, Zhengxiangbai Banner; ZLB, Zhenglan Banner; AB, Abaga Banner; XH, Xinghe County; KT, Hexigten Banner; WU, Wast Ujumuqin Banner; EU, East Ujumuqin Banner.

3. Materials and Methods

3.1. Materials

3.1.1. Soil Moisture Data

Due to the small number of observation stations and uneven spatial distribution of soil water content, the measured data are very limited and cannot meet the research needs, so GLDAS data products are selected. Combining satellite and ground observation data with advanced land surface models and assimilation techniques, the product features optimized near-real-time features that provide important information about land surface and energy flux for scientific research, especially in areas where reliable ground measurements are not possible [33,34]. The Noah model in GLDAS can provide soil moisture, temperature, atmospheric pressure, and other data, but for agricultural drought, soil water content in the root zone can be more accurately evaluated [35]. Soil water content can directly affect the root water absorption and transpiration of crops, which is suitable for the evaluation of agricultural drought [31]. Therefore, this paper selects the monthly time series raster data set of 1960–2021 soil root zone water content obtained via the Noah model in GLDAS V2.0 (spatial resolution is 0.25° × 0.25°) to calculate agricultural drought index (SSMI) at different time scales. On this basis, the temporal and spatial variations and periodic characteristics of agricultural drought at monthly, seasonal, and annual scales in IMIRB were analyzed. The root zone soil Moisture grid dataset was obtained from NASA's Goddard Earth Science Data and Information Services Center (https://disc.gsfc.nasa.gov/datasets/GLDAS_NOAH025_M_2.0/, accessed on 3 November 2023).

3.1.2. Meteorological Factor Data and Drought Statistics

The CRU TS v.4.07 dataset is one of the most widely used climate datasets, produced by the National Centre for Atmospheric Science (NCAS) in the United Kingdom, that provides 0.5° resolution monthly scale data covering the global land surface from 1901 to the present. In this paper, the data of temperature (T), precipitation (P), evapotranspiration (E), and humidity (H) are derived from the CRU TS v.4.07 dataset, and the time scale is

obtained   monthly
(https://crudata.uea.ac.uk/cru/data/hrg/cru_ts_4.07/cruts.2304141047.v4.07/, accessed on 1 November 2023). The data on crop disaster areas and extinct areas in the study area were obtained from China Statistical Yearbook, but due to the limited statistical years of China Statistical Yearbook, only data from 1998 to 2021 were collected (https://www.stats.gov.cn/sj/ndsj/, accessed on 27 November 2023).

3.2. *Methods*

3.2.1. Standardized Soil Moisture Index

Due to the advantages of multiple time scales and strong spatio-temporal continuity, SSMI was selected to characterize agricultural drought in this paper. Previous studies have shown that normal distribution is the optimal distribution for fitting soil water content [26,36]. Therefore, in this paper, the normal distribution is used to fit and calculate the cumulative distribution function of soil water content, and then the cumulative distribution function is standardized to obtain SSMI.

The SSMI is built as follows:

(1) Construct cumulative soil water sequence X at different scales:

$$X_i^k = \sum_{i-k+1}^{i} S_i \tag{1}$$

where i is the month; k is the time scale, and k = 1, 2,… 12, S_i is the soil water content;

(2) The normal distribution function is used to fit the X_i^k sequence and calculate the probability density function $f(x)$ and the cumulative distribution function $F(x)$:

$$f(x) = \frac{1}{\sqrt{2\pi}\sigma} e^{-\frac{(x-\mu)^2}{2\sigma^2}} \tag{2}$$

$$F(x) = \frac{1}{\sqrt{2\pi}\sigma} \int_{-\infty}^{x} e^{-\frac{(x-\mu)^2}{2\sigma^2}} dx \tag{3}$$

where μ is the mean, and σ^2 is the variance;

(3) Standardize $F(x)$ to obtain SSMI:

$$SSMI = W - \frac{C_0 + C_1 + C_2 W^2}{1 + d_1 W + d_2 W^2 + d_3 W^3} \tag{4}$$

$$W = \sqrt{-2\ln(P)} \tag{5}$$

where when $P \leq 0.5$, $P = 1 - F(x)$, and when $P > 0.5$, $P = F(x)$. The other parameters are C_0 = 2.515517, C_1 = 0.802853, C_2 = 0.010328, d_1 = 1.432788, d_2 = 0.189269, and d_3 = 0.001308.

According to the existing research results, the agricultural drought was graded, and −0.5 was selected as the drought threshold [37,38]. Table 1 shows the classification criteria of drought grade.

Table 1. Drought classification of SSMI.

Drought Level	SSMI	Drought Severity
I	−0.5 < SSMI	No drought
II	−1 < SSMI ≤ −0.5	Light drought
III	−1.5 < SSMI ≤ −1	Moderate drought
IV	−2 < SSMI ≤ −1.5	Severe drought
VI	SSMI ≤ −2	Extreme drought

3.2.2. Modified Mann–Kendall Test

MMK trend test can eliminate the autocorrelation components in time series, making the results of the trend test more reliable. This method firstly calculates the estimated

trend value of time series, then calculates the autocorrelation coefficient, then obtains the variance of trend statistics according to the autocorrelation coefficient, and finally calculates the trend value of time series according to the variance and characterizes the change trend of time series and its significance. Many scholars have used this method to study the time variation trend of drought index [39–41]. In this paper, the MMK method is used to analyze the temporal variation trend of SSMI, and it is applied to the grid scale to reveal the spatial distribution characteristics of drought variation trend in IMIRB. See the literature for detailed calculation steps [42].

3.2.3. Three-Dimensional Identification Method of Drought Events

The 3D drought recognition method is the method to extract the drought events from the 3D space (time–longitude–latitude) of the drought index [43]. Drought 3D recognition mainly includes drought patch recognition, drought patch time–history connection, and drought characteristic variable extraction [26].

(1)   Drought patch recognition

Before the identification of drought patches, A minimum drought area threshold (A) should be set in advance. The drought patch recognition method first divides the spatially adjacent grids into categories; that is, the grids (SSMI < −0.5) that have drought at the same time in adjacent locations are classified into one category and marked with the same number, and then they are combined into one drought patch. If there is no other drought grid adjacent to the current drought grid, a number is re-labeled to create the next drought patch, and the steps are repeated until there is no drought grid adjacent area. According to the above method, a number of dry patches with different areas can be obtained and marked with different numbers. If the area of the identified drought patch is smaller than A, it is judged that it does not constitute a drought event, and it is eliminated (A_3 and A_4 in Figure 2). At the same time, this area threshold can also be used to judge the time continuity between drought patches so as to avoid the combination of drought events that were not related or completely unrelated within the next two months, resulting in unsatisfactory identification results [44]. According to the relevant literature, this paper only considers the drought pattern spots whose area is larger than 1.6% of the whole study area [45–47];
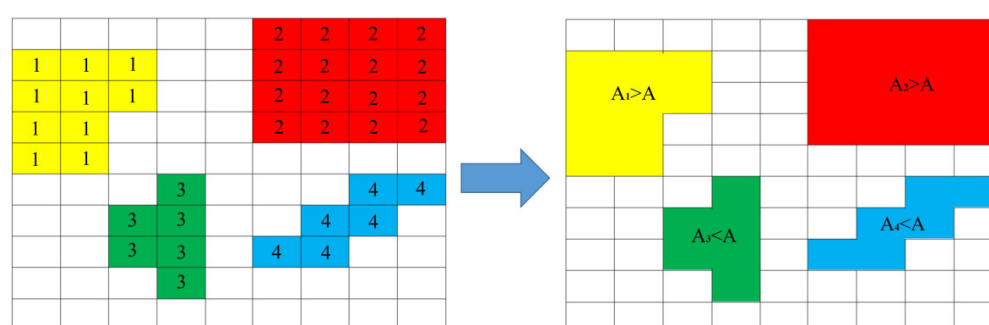

Figure 2. Schematic diagram of drought patch recognition.

(2)   Drought patch time–history connection

For the identified dry patches, it is determined whether there is a connection between the dry patches in time and whether it constitutes a continuous drought event. For example, in A_3 and A_4 of Figure 3, if the coincidence area (A^*) between a certain dry patch A_t and a certain dry patch A_{t+1} at an adjacent time is greater than the threshold value A, then A_t and A_{t+1} are considered to be continuous in time, and it is determined that they belong to the same drought event; otherwise, it did not belong to the same drought event. According to this rule, the overlapping area between any pair of drought patches at two adjacent moments is judged, in turn, from the first month until the overlapping area is less

than a, and the drought patches identified as belonging to the same drought event are assigned the same number. The above steps are repeated to connect the longitude and latitude drought patches in the time course to form a spatio-temporal connected drought index continuum and obtain multiple three-dimensional drought events;
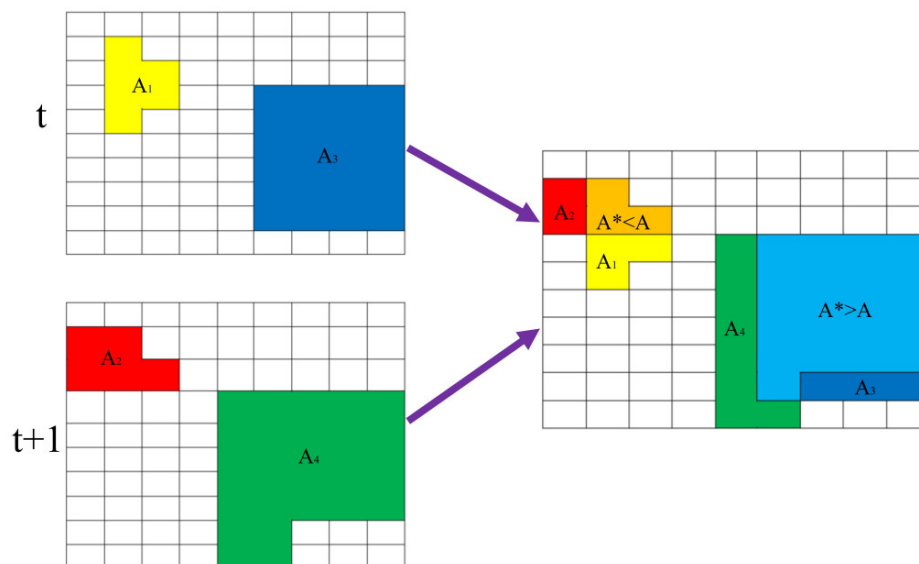

Figure 3. Schematic diagram of time–history connection of arid patches.

(3) Drought characteristic variable extraction.

Compared with the two-dimensional recognition method, the drought features extracted based on the three-dimensional recognition method are more complex and can more comprehensively reflect the spatio-temporal continuous evolution characteristics. Compared with the traditional results of drought identification, this method can extract more characteristic variables reflecting the dynamic change in drought space. This paper analyzes the continuous spatio-temporal evolution characteristics of a single drought event and the development law of regional drought from five drought characteristic variables: drought duration, area, severity, center, and migration direction.

(1) Drought duration is the duration of the drought event; it is the first and the last time interval between dry patches; it can also be considered a drought at the height of the three-dimensional continuum;
(2) Drought area is the vertical projection area of the three-dimensional continuum of drought on a two-dimensional plane (longitude × latitude);
(3) Drought severity is the sum of the water shortage degree of all arid bodies, that is, the volume of the three-dimensional drought continuum;
(4) Drought center is a drought three-dimensional continuum center of mass;
(5) Drought migration direction is a drought three-dimensional continuum drought center at every moment.

3.2.4. Cross-Wavelet Transform

The cross-wavelet transform reveals the two signals in time-frequency distribution on the related degree [48]. Detailed definitions and calculations can be found in [49]. In this paper, the dynamic relationship between SSMI and meteorological factors was investigated via the cross-wavelet method, and the driving effect of meteorological factors on IMIRB agricultural drought was revealed. Suppose that the continuous wavelet transforms of two-time series X = (x_1, x_2,… x_n) and Y = (y_1, y_2,… y_n) are $W_n^x(s)$ and $W_n^y(s)$; then, the cross-wavelet transform between them is

$$W_n^{xy}(s) = W_n^x(s) * W_n^{y*}(s) \tag{6}$$

where $W_n^{y*}(s)$ represents the complex conjugation of $W_n^y(s)$, and s represents the delay.

4. Results

4.1. Temporal Evolution Characteristics of Agricultural Drought

4.1.1. Characteristics of Drought Time Evolution in Multi-Scale Agriculture

The fluctuations of SSMI on different time scales can reflect the drought effects of different cumulative periods in the past. For example, SSMI-1, SSMI-3, SSMI-12, and SSMI-24 reflect the drought conditions in the past month, quarter, year, and two years, respectively. In this paper, the SSMI time series of 1–24 months in IMIRB in the last 60 years is calculated, and the heat map is drawn to depict the temporal variation characteristics of the agricultural drought index at multiple scales (Figure 4). The light color indicates that the larger SSMI value means the lighter drought degree, and the dark color indicates that the smaller SSMI value means the heavier drought degree. As can be seen from Figure 4, agricultural droughts are a gradual process in time evolution, and when the time scale is short, dry and wet alternate frequently. With the increase in time scale, the fluctuation of drought decreases, and the periods of drought and wetting increase significantly, which means that the number of droughts decreases while the duration and intensity of droughts increase. Under different time scales, the SSMI in IMIRB showed a decreasing trend before 1968 and from 2001 to 2014; that is, the drought showed an increasing trend. The SSMI showed an upward trend from 1968 to 2000 and from 2015 to now; that is, the drought showed a weakening trend. It can also be seen in Figure 4 that relatively serious agricultural droughts occurred in IMIRB around 1967, around 2002, and from 2005 to 2012. In other periods, droughts and floods appeared alternately, and humidification was the main factor.
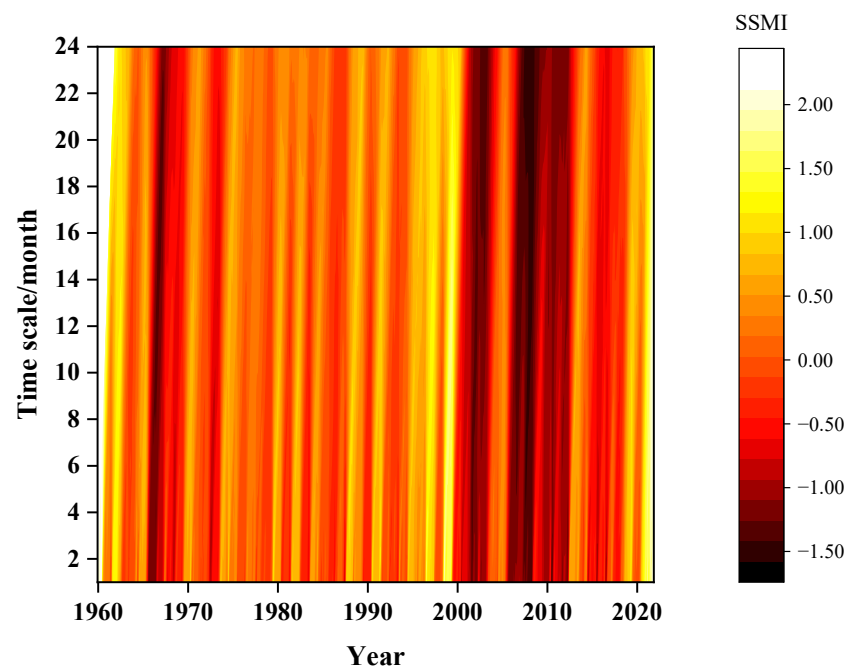
Figure 4. Temporal evolution characteristics of multi-scale SSMI in IMIRB from 1960 to 2021.

4.1.2. Variation Trend of Agricultural Drought Time at Different Scales

The temporal variation characteristics of monthly, seasonal, and annual scales SSMI of IMIRB are shown in Figure 5. Among them, the SSMI index at all scales showed a downward trend. From the perspective of the monthly scale, the linear tendency rate of SSMI

was close to 0, and the drought trend was small. From the annual scale, the linear tendency rate of SSMI was −0.063/10a, and it developed toward drought, and the change trend in each period was roughly the same as that in the monthly scale. SSMI showed a decreasing trend in all seasons, and the change trend in spring was the largest. From the multi-year trend, all seasons showed an arid trend. In addition, the change trend of SSMI in different seasons was consistent, with alternating upward and downward trends. SSMI of each season showed a downward trend in the 1960s, showing the characteristics of drought, and showed an upward trend of fluctuation from 1970 to 2000; that is, drought showed a weakening trend. It reached the maximum value around 1998 and showed a downward trend in the 2000s, which showed the characteristics of drought. After 2015, the SSMI of each season showed a rapid upward trend, and the wetting trend in summer during this period was significant.
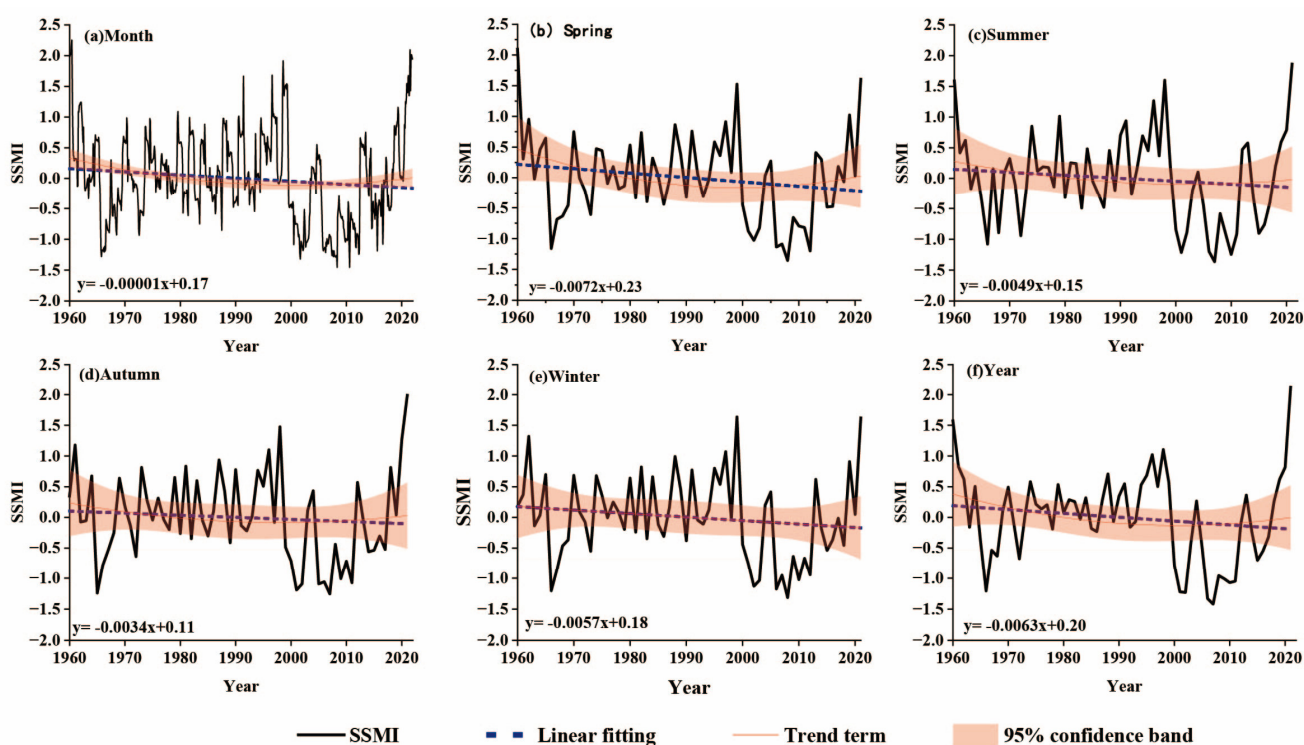
Figure 5. Monthly, seasonal, and annual scales SSMI time trends in IMIRB from 1960 to 2021. (**a**) Month. (**b**) Spring. (**c**) Summer. (**d**) Autumn. (**e**) Winter. (**f**) Year.

4.1.3. Temporal Characteristics of Seasonal Drought Intensity and Area Proportion

As can be seen in Figure 6, the variation characteristics of drought area proportion and intensity in the IMIRB were similar in four seasons. The drought area proportion and intensity in four seasons around 1966 and the 2000s were relatively large, and the drought intensity of other seasons fluctuated around 0.75 in 1968–1990 except for summer. Since 2000, the spring drought in the study area has been characterized by high intensity, strong persistence, and significant drought. There were the most years without drought in summer, which was weaker than the other three seasons. The correlation between autumn and winter was great, and the maximum drought intensity could reach 1.5; the maximum drought area accounted for 95%, and the drought influence of the two seasons was greater.
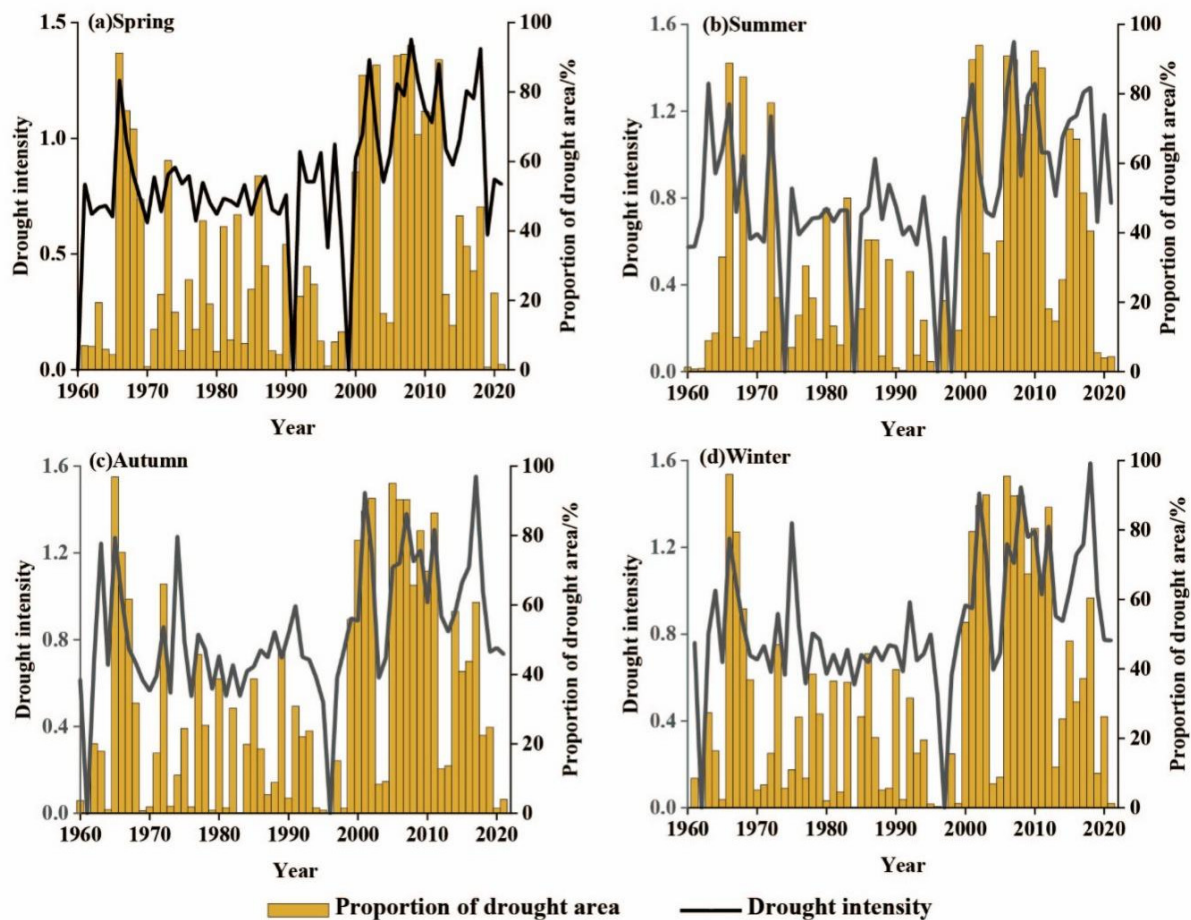
Figure 6. Variation characteristics of seasonal drought intensity and area proportion in IMIRB from 1960 to 2021. (**a**) Spring. (**b**) Summer. (**c**) Autumn. (**d**) Winter.

4.2. Spatial Evolution Characteristics of Agricultural Drought

4.2.1. Spatial Distribution Characteristics of Drought Change Trend

Figure 7 shows the spatial distribution characteristics of seasonal SSMI change trends based on the MMK trend test. On the whole, the four seasons of drought trend distribution characteristics of IMIRB were similar. The regions where SSMI showed a significant downward trend were concentrated in the middle and northwest of IMIRB, and the regions where SSMI showed an upward trend were concentrated in the east and west of IMIRB. The specific characteristics of each season are as follows: compared with other seasons, the area of spring showed a significant decline trend, accounting for 35.40%, and the SSMI also showed a decline trend in the northeastern part of Abaga Banner (AB), the northern part of Silinghot City (XH), and the western part of Eastern Ujamuqin Banner (EU). In summer, there are fewer areas in IMIRB where SSMI showed a significant upward trend than in other seasons. In autumn, the area of SSMI in IMIRB showed a significant downward trend, accounting for 26.46%. The spatial distribution of SSMI in IMIRB in winter was roughly the same as that in autumn. Compared with autumn, SSMI in the eastern part of AB and the western part of EU showed a downward trend in winter.

4.2.2. Spatial Distribution Characteristics of Agricultural Drought Intensity

Figure 8 shows that the drought intensity of IMIRB in four seasons is concentrated between 0.68 and 1.47. In this paper, the regions with agricultural drought intensity less than 1 are defined as low-value regions, and those with agricultural drought intensity

greater than 1.2 are defined as high-value regions. The high-intensity area and low-intensity area of agricultural drought are different in different seasons. Specifically, the area of high agricultural drought intensity in spring was relatively small, and the area of low agricultural drought intensity was larger. The low- and high-value areas of agricultural drought intensity in summer were most concentrated in the northeastern and central parts of IMIRB, respectively. The high-value and low-value areas of autumn drought were distributed in the east and middle of IMIRB, respectively. In winter, the area of high-intensity drought was the largest, but the western region was in the low-intensity area.
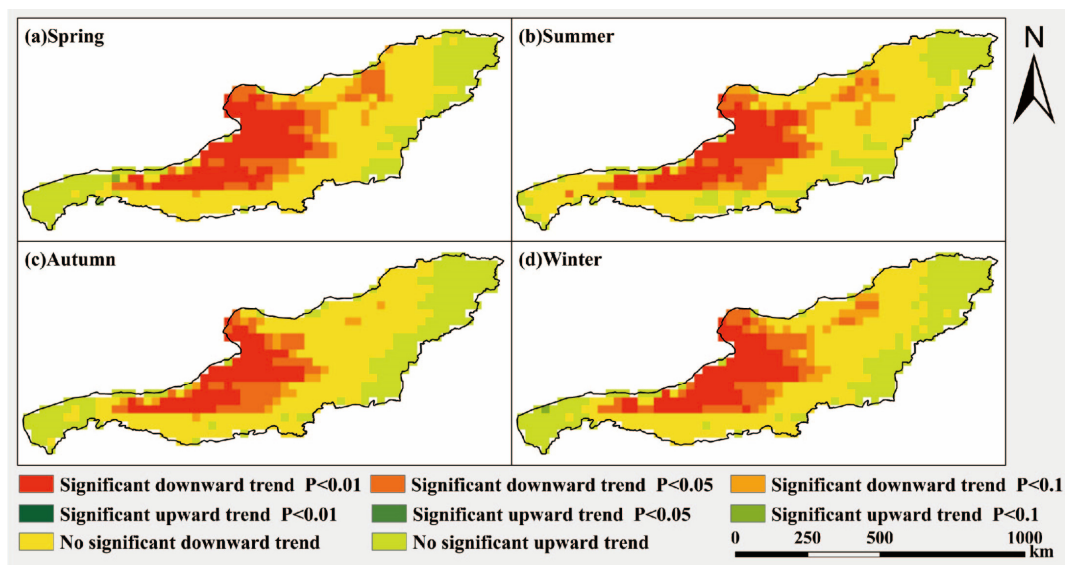
Figure 7. Spatial distribution characteristics of seasonal SSMI trends in IMIRB. (**a**) Spring. (**b**) Summer. (**c**) Autumn. (**d**) Winter.
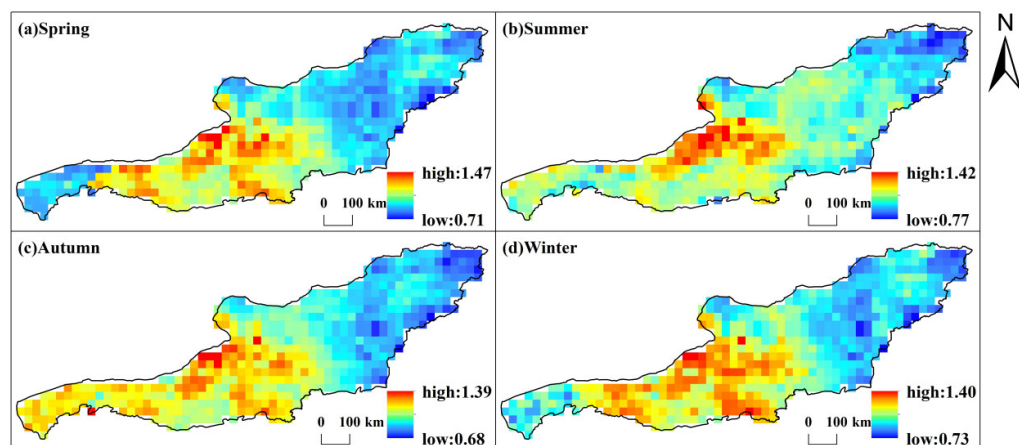
Figure 8. Spatial distribution characteristics of seasonal drought intensity of IMIRB during 1960–2021. (**a**) Spring. (**b**) Summer. (**c**) Autumn. (**d**) Winter.

4.2.3. Spatial Distribution Characteristics of Agricultural Drought Frequency

As shown in Figure 9, the frequency of agricultural drought in most areas of IMIRB in four seasons was mainly maintained between 30% and 35%. Therefore, regions with drought frequency of less than 30% were defined in this paper as low-value regions, while those with drought frequency greater than 35% were high-value regions. Specifically, the high-frequency areas of spring agricultural drought were widely distributed, accounting for 42.70%, including the south of West Ujumuqin Banner (WU), the south of Zhenglan Banner (ZLB), and the west of Urat Rear Banner (UBB). In summer, the agricultural

drought low-frequency area was the widest, accounting for 22.99%, which was widely distributed in the central and western parts of IMIRB. The high-frequency area of autumn drought was larger in the four seasons, and the drought frequency was higher in the central and northeastern parts of IMIRB. Compared with autumn, the high-frequency area of agricultural drought in winter was greatly reduced, and the low-frequency area was more widely distributed.
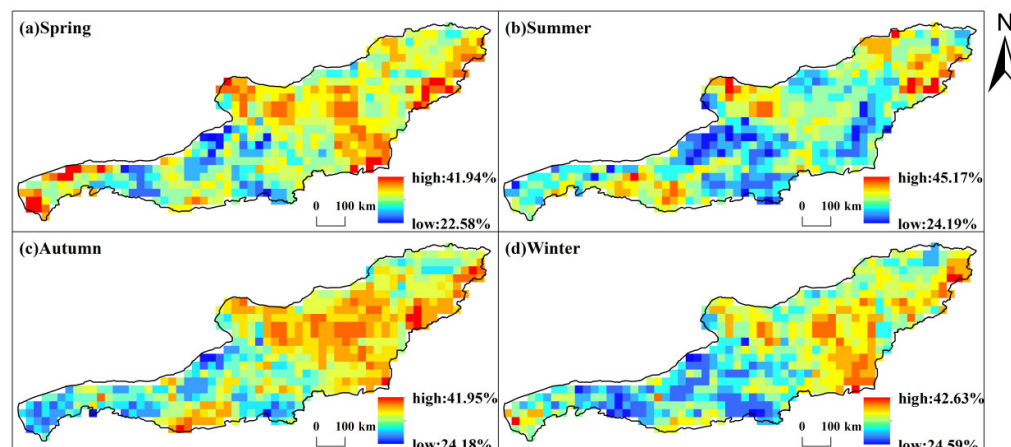

Figure 9. Spatial distribution characteristics of seasonal drought frequency in IMIRB from 1960 to 2021. (**a**) Spring. (**b**) Summer. (**c**) Autumn. (**d**) Winter.

4.3. Dynamic Evolution of Agricultural Drought Events Based on Three-Dimensional Recognition Method

4.3.1. Drought Recognition Results Based on Three-Dimensional Recognition Method

Based on the three-dimensional recognition method, SSMI-3 was used to identify 85 agricultural drought events in the study area from 1960 to 2021, accounting for 11.61% of the total number of months, among which 34 drought events lasted at least two months. According to the order of drought severity, the most serious in the first 10 games, specific features of agricultural drought events, and variables are listed in Table 2, where the number represents the serial number of each drought event determined in chronological order among the 85 drought events. The duration of these 10 drought events lasted at least eight months. Among them, the 36th agricultural drought event occurred from October 2000 to May 2002, which was the most serious, with a drought severity of 3.528×10^6 months·km² and a drought area of 2.419×10^5 km². The longest durations of the 5th (August 1965–June 1966) and 59th (September 2008–July 2009) drought events were 11 months, ranking 4th and 8th, respectively. The 51st drought event lasted 9 months, from September 2006 to May 2007, with a drought severity of 1.089×10^6 months·km² and a drought area of 1.407×10^5 km².

Table 2. The 10 worst agricultural drought events, 1960–2021.

Number	Start Time (Month Year)	End Time (Month Year)	Drought Duration (Month)	Drought Center		Drought Area (10^4 km²)	Drought Severity (10^5 months·km²)
				Lon	Lat		
36	October 2020	May 2002	20	113.81	43.20	24.19	35.28
56	October 2007	June 2008	9	114.52	43.73	26.31	27.58
83	July 2017	August 2018	14	111.09	42.51	12.99	23.12
5	August 1965	June 1966	11	111.80	42.31	16.85	18.99
45	September 2005	May 2006	9	114.44	43.89	19.40	18.32
69	September 2011	June 2012	10	112.43	42.68	14.62	18.20
61	September 2009	May 2010	9	114.69	43.58	17.43	16.59

59	September 2008	July 2009	11	115.84	44.58	16.84	15.17
41	October 2002	May 2003	8	112.38	42.64	13.71	11.63
51	September 2006	May 2007	9	111.76	42.59	14.07	10.89

4.3.2. Analysis of Typical Agricultural Drought Events

Taking the most severe drought event (No. 36) as a typical agricultural drought event, Figure 10 shows the three-dimensional perspective of the spatio-temporal changes in the event and the time trend of the characteristic variables. As one can see from Figure 10, the monthly trends of drought area and severity of No. 36 were basically the same, showing an upward trend from October 2000 to May 2001, reaching a maximum value in May 2001 (7.99×10^4 km^2 and 1.17×10^5 months·km^2, respectively) and then showing a downward trend in the next month. From June 2001 to September 2001, it showed a significant upward trend and reached the maximum in September 2001. The drought area and drought severity were 2.26×10^5 km^2 and 3.61×10^5 months·km^2, respectively. From October 2001 to May 2002, the drought area and drought severity showed downward trends and reached a minimum in May 2002, with the drought area and drought severity of 9.62×10^4 km^2 and 1.39×10^5 months·km^2, respectively.
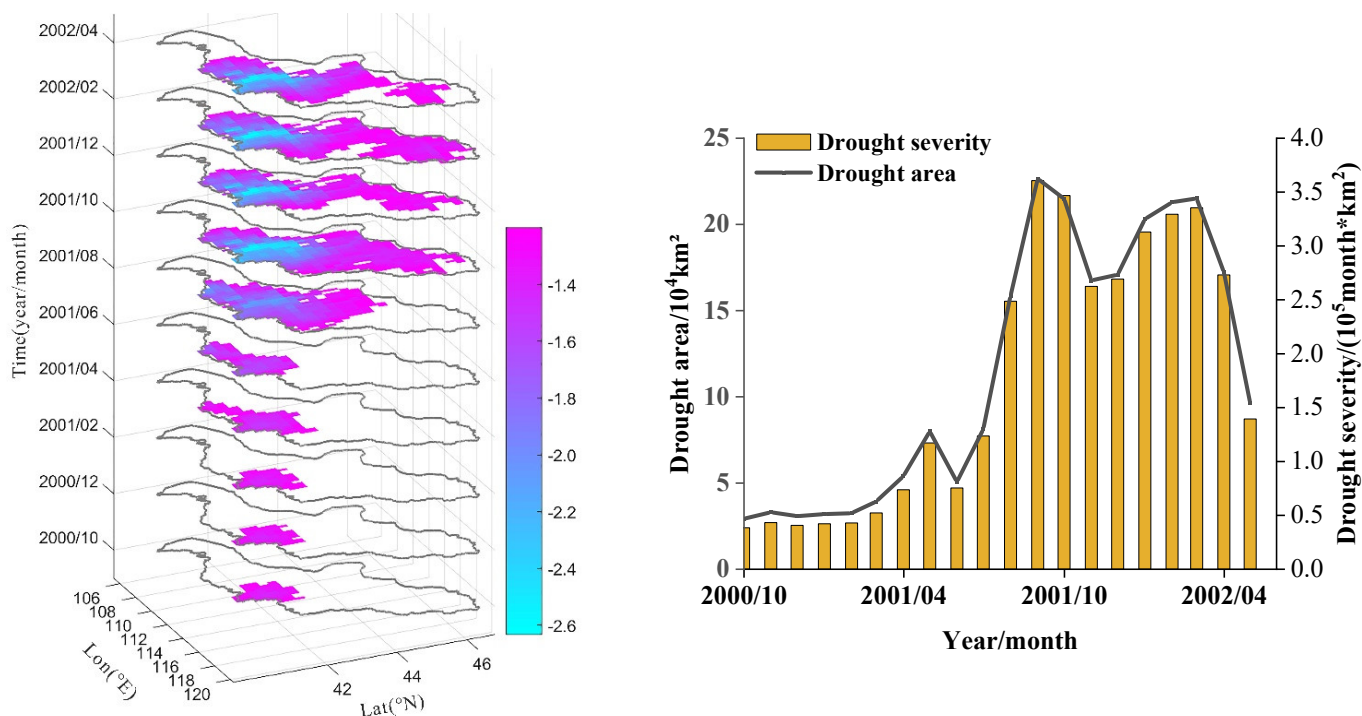
Figure 10. Three-dimensional perspective of the 36th agricultural drought and temporal trend of characteristic variables.

Taking this typical agricultural drought event as an example, Figure 11 analyzes the spatio-temporal dynamic evolution process from the beginning to the end of the drought, and Figure 12 analyzes the central migration path of the drought event. This agricultural drought event lasted 20 months from October 2000 to May 2002, with a drought severity of 3.528×10^6 months·km^2, ranking first among all agricultural drought events. Its spatio-temporal dynamic evolution and migration process were relatively simple, with specific characteristics as follows: the agricultural drought began in October 2000, with an area of 2.92×10^4 km^2, covering the western part of Zhengxiangbai Banner (ZB), the southern part of Sunid Right Banner (SRB), Xianghuang Banner (XB), Shangdu County (SD), Xinghe County (XH), and Qahar youqi houqi (CRW). The drought center was located in the southern part of SRB. In September 2001, the drought area expanded rapidly to 2.26×10^5 km^2,

and the drought center moved southeast to the southern part of Sunid Left Banner (SLB). Except for the western and northeastern parts of IMIRB, other regions suffered from drought, and the northwestern part of EU and the central part of WU suffered the most severe drought. In November, the drought area and severity decreased to 1.68×10^5 km^2 and 2.63×10^5 months·km^2, respectively, and the drought center moved from the southeast to the west of AB. In March 2002, the drought severity increased, and the drought area was 2.15×10^5 km^2, concentrated in the northeastern and central regions. Subsequently, the drought was alleviated. In May 2002, the drought area was reduced to 9.62×10^4 km^2; the drought situation was weakened, and the drought event was lifted.
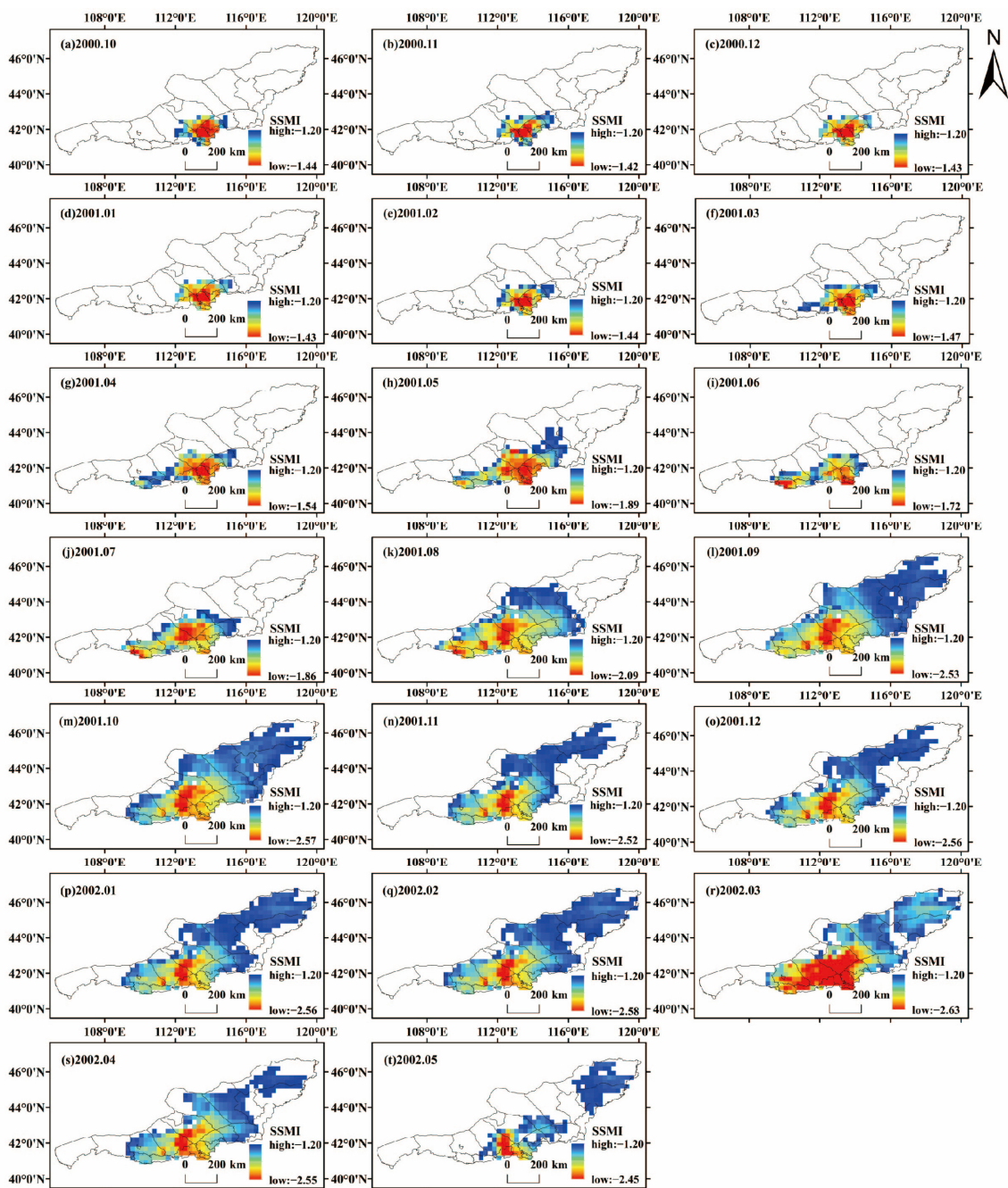
Figure 11. Temporal and spatial dynamic evolution of typical agricultural drought events (**a–t**): October 2000–May 2002.
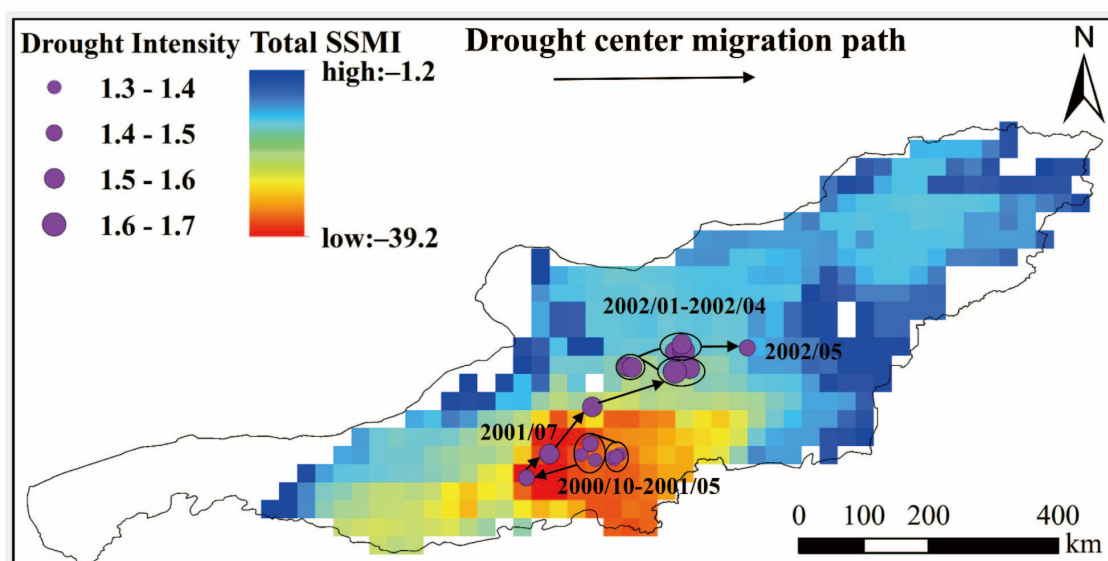
Figure 12. Migration path of typical agricultural drought center.

5. Discussion

5.1. Driving Factor Analysis

The cross-wavelet energy spectrum and condensation spectrum of SSMI with T, P, E, and H are shown in Figure 13. It can be seen from Figure 13a that there is no obvious correlation between SSMI and T in the high-energy region, and the three significant resonance periods all show non-positive correlation, which are 1–2 years from 1964 to 1967, 4–5 years from 1999 to 2005, and 7–8 years from 2005 to 2013, respectively. As can be seen from Figure 13b, there is only a significant resonance period of 1–2 years between 1987 and 1993, and the correlation between the two is low. Figure 13c is the cross-wavelet energy spectrum of SSMI and P. It can be seen from the figure that there is a certain correlation between them, in which there is a significant resonance period of 2–3 years in 1964–1967 and a significant resonance period of 4–8 years in 1997–2011, all of which are approximately positive correlations. As can be seen from Figure 13d, SSMI and P mainly have four significant resonance periods in the low-energy region, among which there are 1–8 years of significant resonance periods in 1964–1983, 16–20 years in 1982–2002, 3–10 years in 1993–2015, and 1–2 years in 1996–2002. Figure 13e,f shows the cross-wavelet energy spectra and condensation spectra of SSMI and E, respectively. Both figures show that there is a significant resonance period of 4–5 years from 2000 to 2005, and it tends to be negatively correlated. As can be seen from Figure 13g, SSMI and H only had a significant resonance period of 4–6 years from 2000 to 2010, mainly in a positive correlation. Figure 13h shows that SSMI and H mainly have three significant resonance periods in the low-energy region, among which a significant resonance period of 1–3 years existed from 1965 to 1985; 3–6 years existed from 1985 to 2010, and 1–2 years existed from 1995 to 2000.
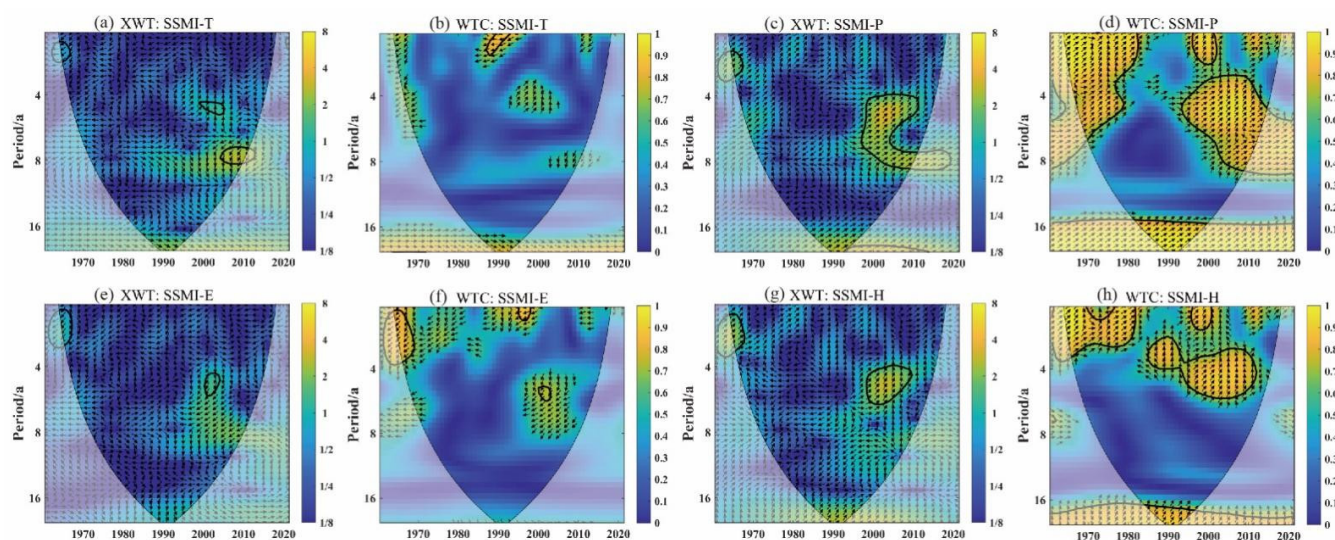
Figure 13. Cross-wavelet energy spectrum and condensation spectrum of SSMI with T, P, E, and H. (**a**) XWT: SSMI-T; (**b**) WTC: SSMI-T; (**c**) XWT: SSMI-P; (**d**) WTC: SSMI-P; (**e**) XWT: SSMI-E; (**f**) WTC: SSMI-E; (**g**) XWT: SSMI-H; (**h**) WTC: SSMI-H.

This paper analyzed the influence of T, P, E, H, and other meteorological factors on SSMI using the cross-wavelet method and found that T and E were negatively correlated with it, but P and H were positively correlated with it. All four meteorological factors have certain driving effects on agricultural drought, and P has a greater influence on drought and a stronger correlation. Agriculture depends on rainfall, and when it is not sufficient, it leads to crop failure [50]. Miao et al. identified that P is the main driving factor of vegetation growth that can reduce the possibility of drought disasters when analyzing drought characteristics and influencing factors in Inner Mongolia [51]. Guo et al. also pointed out that precipitation in Northern China can slow down drought and has a positive impact on it, which plays a dominant role in the dynamic characteristics of drought [52]. It is worth noting that the cross-wavelet energy spectrum and condensation spectrum of the four meteorological factors and SSMI all have significant resonance periods of different time scales in the 21st century, which corresponds to the above research results, indicating that agricultural drought has occurred frequently and with high intensity since the 21st century.

5.2. Advantages and Limitations

With global warming, the problem of drought in IMIRB has become more and more serious, and many scholars have studied the drought problem in this region [20,30,53,54]. An et al. analyzed the drought characteristics and changing trend of Inner Mongolia based on SPEI and showed that the areas with strong drought intensity were distributed in the north-central and western regions [20]. Existing studies showed that drought was more serious in the western region, which is similar to this study's research results. The main reason is that the western region is dominated by desertification grassland, and the rainfall is scarce. It takes a long time and is difficult to recover after the drought, so the drought in the western region shows the characteristics of high intensity. Based on the SSMI index, this study identified the spatio-temporal evolution characteristics of agricultural drought events in IMIRB from 1960 to 2021 and found that the SSMI index of all scales showed a downward trend and showed the characteristics of drought, which was similar to the research result of Zhao et al., indicating that climate warming led to more severe drought situation [55]. At the same time, the research results showed that the 2000s SSMI in this region showed a downward trend, and the drought was the most severe around 2007, and then the SSMI showed an upward trend, and the drought was alleviated, indicating that the drought had phased characteristics, which is in good agreement with the existing research results [56]. On a spatial scale, Zhang et al. found that the area with an upward

trend of drought was more than the area with a downward trend in Inner Mongolia, and Wang et al. showed that the drought intensification trend was most significant in the northern central part of IMIRB [57,58]. The research results of this paper support the above viewpoint and show that the area with a significant increase in spring drought is the largest, and drought is also the most prone to occur, which deepens the previous research results.

The above studies used a one-dimensional or two-dimensional scale to identify drought events and characterized drought from the aspects of drought duration, drought frequency, drought intensity, etc., but failed to identify drought variables such as drought center and drought migration path, resulting in the loss of some drought characteristic variables, and, thus, unable to comprehensively and accurately analyze its spatio-temporal evolution characteristics and dynamic evolution laws. In this paper, the agricultural drought events in IMIRB are identified from a three-dimensional perspective, and the drought characteristic variables of each drought event are obtained so that the spatio-temporal and dynamic evolution laws of each agricultural drought event could be intuitively recognized according to drought characteristic variables such as drought duration, intensity, drought center, and migration path. According to the results of three-dimensional identification, 9 of the 10 most serious agricultural drought events from 1960 to 2021 were in 2000–2021, and the most serious drought event began in October 2000 and ended in May 2002. At the same time, as can be seen from Figure 14, in 2000–2010 and 2015–2018, there were more areas affected by crops and areas of crop failure, reflecting the serious agricultural drought during this period. This is very similar to the results identified by the three-dimensional identification method, indicating that the three-dimensional identification method can be used to identify agricultural drought and its characteristic variables.
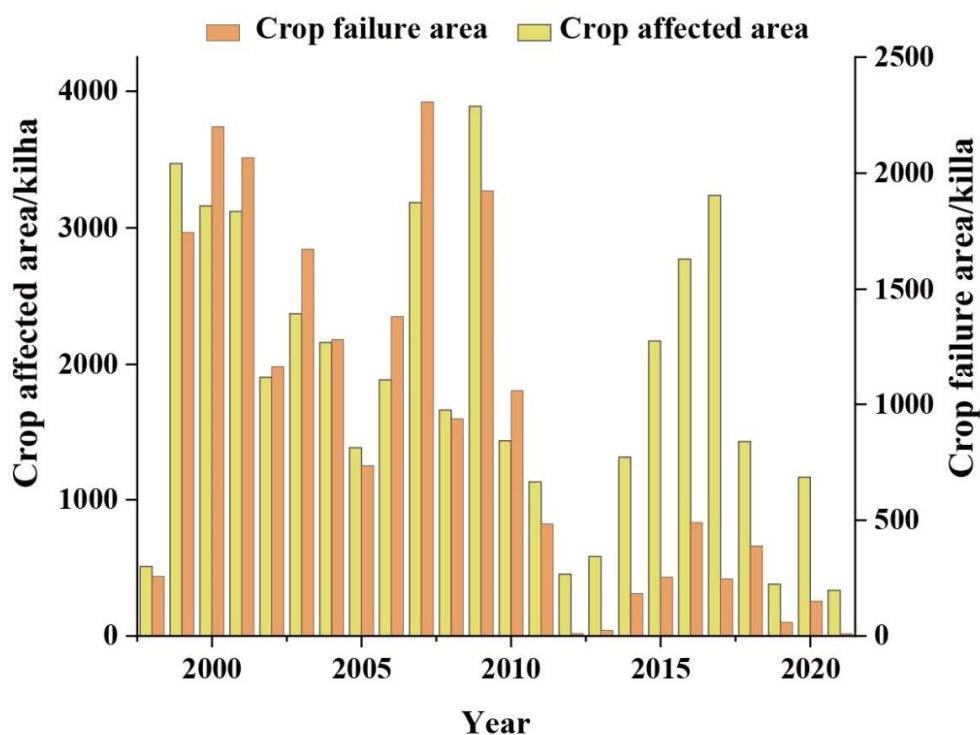

Figure 14. The affected area of crops and the area of crop failure from 1998 to 2021.

However, there are still some limitations in this study. In this paper, a monthly time series raster data set of soil root zone water content with a resolution of 0.25° × 0.25° was selected to calculate SSMI at different time scales. The raster accuracy is a little coarse, which leads to insufficient data accuracy and cannot fully and accurately reflect the soil root zone water content in various locations in the study area. Therefore, the agricultural

drought index calculated on the basis of soil root zone water content may be somewhat different from the actual situation. In addition, when we calculate the agricultural drought index, we only consider the soil water content but do not consider the impact of human activities on drought. In fact, human activities can lead to changes in land types and also affect the division of dry areas [26]. Finally, this paper only studies the influence of four meteorological factors on agricultural drought and does not consider the influence of other meteorological factors, human activities, and underlying surface factors. In future studies, the effects of other factors on agricultural drought should be considered, and it is suggested that the drought center and migration path of each agricultural drought should be identified comprehensively and deeply, and the spatio-temporal dynamic law of agricultural drought should be understood so as to formulate corresponding drought prevention and relief programs.

6. Conclusions

This paper uses SSMI to characterize the agricultural drought in IMIRB from 1694 to 2021 and analyzes its temporal and spatial evolution characteristics. Then, the drought events are identified via the three-dimensional identification method, and the drought characteristic variables of typical drought events are extracted, revealing the development law of typical drought events. Finally, the influence of T, P, E, and H on SSMI is analyzed using the cross-wavelet method. This paper draws the following conclusions:

(1) With the increase in time scale, the fluctuation of agricultural drought decreased, but the SSMI index of all scales showed a downward trend, and the spring drought was the most obvious (linear tendency rate was −0.072/10a), and the change trend of drought area proportion and intensity was similar in four seasons;

(2) The spatial distribution characteristics of drought change trend in four seasons were similar, but the area with a significant downward trend of drought in spring was the largest, and the area of the high-frequency region was also the largest, accounting for 35.40% and 42.70% respectively;

(3) The most serious agricultural drought happened from October 2000 to May 2002, and both the drought area and severity reached the maximum in September 2001, with the drought area and intensity of 2.26×10^5 km^2 and 3.61×10^5 months·km^2, respectively. The drought event mainly experienced five processes: drought onset–intensification–decay–re-intensification–termination, and the migration path of the drought center was characterized by southwest to northeast transmission;

(4) T, P, E, and H all played a driving role in the occurrence of agricultural drought. T and E were mainly negatively correlated with SSMI; P and H were mainly positively correlated with SSMI, and P had a greater impact on SSMI.

Author Contributions: Conceptualization, Z.Z. and H.G.; data interpretation and methodology, H.G. and K.F.; validation, K.F.; software, J.L.; original draft preparation, H.G.; funding acquisition, K.F., F.W. and W.Z. All authors have read and agreed to the published version of the manuscript.

Data Availability Statement: Publicly available datasets were analyzed in this study. This data can be found here: [https://disc.gsfc.nasa.gov/datasets/GLDAS_NOAH025_M_2.0/, accessed on 3 November 2023].

Conflicts of Interest: The authors declare no conflicts of interest.

References

1. Zhang, Z.; Wang, Z.; Lai, H.; Wang, F.; Li, Y.; Feng, K.; Qi, Q.; Di, D. Lag Time and Cumulative Effects of Climate Factors on Drought in North China Plain. *Water* **2023**, *15*, 3428. https://doi.org/10.3390/w15193428.

2. Deo, R.C.; Byun, H.-R.; Adamowski, J.F.; Begum, K. Application of effective drought index for quantification of meteorological drought events: A case study in Australia. *Theor. Appl. Climatol.* **2017**, *128*, 359–379.

3. Li, Y.; Xie, Z.; Qin, Y.; Xia, H.; Zheng, Z.; Zhang, L.; Pan, Z.; Liu, Z. Drought under global warming and climate change: An empirical study of the Loess Plateau. *Sustainability* **2019**, *11*, 1281.

4. Pritchard, H.D. Asia's glaciers are a regionally important buffer against drought. *Nature* **2017**, *545*, 169–174.

5. Lesk, C.; Rowhani, P.; Ramankutty, N. Influence of extreme weather disasters on global crop production. *Nature* **2016**, *529*, 84–87.

6. Zhu, Y.; Liu, Y.; Wang, W.; Singh, V.P.; Ma, X.; Yu, Z. Three dimensional characterization of meteorological and hydrological droughts and their probabilistic links. *J. Hydrol.* **2019**, *578*, 124016.

7. Ling, M.; Guo, X.; Shi, X.; Han, H. Temporal and spatial evolution of drought in Haihe River Basin from 1960 to 2020. *Ecol. Indic.* **2022**, *138*, 108809.

8. Tigkas, D.; Vangelis, H.; Proutsos, N.; Tsakiris, G. Incorporating aSPI and eRDI in drought indices calculator (DrinC) software for agricultural drought characterisation and monitoring. *Hydrology* **2022**, *9*, 100.

9. Kazemzadeh, M.; Malekian, A. Spatial characteristics and temporal trends of meteorological and hydrological droughts in northwestern Iran. *Nat. Hazards* **2016**, *80*, 191–210.

10. Mishra, A.K.; Singh, V.P. A review of drought concepts. *J. Hydrol.* **2010**, *391*, 202–216.

11. Parmesan, C.; Morecroft, M.D.; Trisurat, Y. *Climate Change 2022: Impacts, Adaptation and Vulnerability*; Intergovernmental Panel on Climate Change: Geneva, Switzerland, 2022.

12. Mirzabaev, A.; Kerr, R.B.; Hasegawa, T.; Pradhan, P.; Wreford, A.; von der Pahlen, M.C.T.; Gurney-Smith, H. Severe climate change risks to food security and nutrition. *Clim. Risk Manag.* **2023**, *39*, 100473.

13. Dai, M.; Huang, S.; Huang, Q.; Leng, G.; Guo, Y.; Wang, L.; Fang, W.; Li, P.; Zheng, X. Assessing agricultural drought risk and its dynamic evolution characteristics. *Agric. Water Manag.* **2020**, *231*, 106003.

14. Potopová, V.; Štěpánek, P.; Možný, M.; Türkott, L.; Soukup, J. Performance of the standardised precipitation evapotranspiration index at various lags for agricultural drought risk assessment in the Czech Republic. *Agric. For. Meteorol.* **2015**, *202*, 26–38.

15. Qin, Y.; Yang, D.; Lei, H.; Xu, K.; Xu, X. Comparative analysis of drought based on precipitation and soil moisture indices in Haihe basin of North China during the period of 1960–2010. *J. Hydrol.* **2015**, *526*, 55–67.

16. Winkler, K.; Gessner, U.; Hochschild, V. Identifying droughts affecting agriculture in Africa based on remote sensing time series between 2000–2016: Rainfall anomalies and vegetation condition in the context of ENSO. *Remote Sens.* **2017**, *9*, 831.

17. Martínez-Fernández, J.; González-Zamora, A.; Sánchez, N.; Gumuzzio, A. A soil water based index as a suitable agricultural drought indicator. *J. Hydrol.* **2015**, *522*, 265–273.

18. Mao, Y.; Wu, Z.; He, H.; Lu, G.; Xu, H.; Lin, Q. Spatio-temporal analysis of drought in a typical plain region based on the soil moisture anomaly percentage index. *Sci. Total Environ.* **2017**, *576*, 752–765.

19. Andreadis, K.M.; Clark, E.A.; Wood, A.W.; Hamlet, A.F.; Lettenmaier, D.P. Twentieth-century drought in the conterminous United States. *J. Hydrometeorol.* **2005**, *6*, 985–1001.

20. An, Q.; He, H.; Nie, Q.; Cui, Y.; Gao, J.; Wei, C.; Xie, X.; You, J. Spatial and temporal variations of drought in Inner Mongolia, China. *Water* **2020**, *12*, 1715.

21. Du, E.; Chen, F.; Jia, H.; Wang, L.; Yang, A. Spatiotemporal evolution and hysteresis analysis of drought based on rainfed-irrigated arable land. *Remote Sens.* **2023**, *15*, 1689.

22. Chen, X.; Li, F.-w.; Li, J.-z.; Feng, P. Three-dimensional identification of hydrological drought and multivariate drought risk probability assessment in the Luanhe River basin, China. *Theor. Appl. Climatol.* **2019**, *137*, 3055–3076.

23. Lloyd-Hughes, B. A spatio-temporal structure-based approach to drought characterisation. *Int. J. Climatol.* **2012**, *32*, 406–418.

24. Guo, H.; Bao, A.; Ndayisaba, F.; Liu, T.; Jiapaer, G.; El-Tantawi, A.M.; De Maeyer, P. Space-time characterization of drought events and their impacts on vegetation in Central Asia. *J. Hydrol.* **2018**, *564*, 1165–1178.

25. Wen, X.; Tu, Y.-h.; Tan, Q.-f.; Li, W.-y.; Fang, G.-h.; Ding, Z.-y.; Wang, Z.-n. Construction of 3D drought structures of meteorological drought events and their spatio-temporal evolution characteristics. *J. Hydrol.* **2020**, *590*, 125539.

26. Feng, K.; Yan, Z.; Li, Y.; Wang, F.; Zhang, Z.; Su, X.; Wu, H.; Zhang, G.; Wang, Y. Spatio-temporal dynamic evaluation of agricultural drought based on a three-dimensional identification method in Northwest China. *Agric. Water Manag.* **2023**, *284*, 108325.

27. Wei, Y.; Zhu, L.; Chen, Y.; Cao, X.; Yu, H. Spatiotemporal variations in drought and vegetation response in Inner Mongolia from 1982 to 2019. *Remote Sens.* **2022**, *14*, 3803.

28. Wang, Y.; Liu, G.; Guo, E. Spatial distribution and temporal variation of drought in Inner Mongolia during 1901–2014 using Standardized Precipitation Evapotranspiration Index. *Sci. Total Environ.* **2019**, *654*, 850–862.

29. Ma, Z.-C.; Sun, P.; Zhang, Q.; Hu, Y.-Q.; Jiang, W. Characterization and evaluation of MODIS-derived crop water stress index (CWSI) for monitoring drought from 2001 to 2017 over Inner Mongolia. *Sustainability* **2021**, *13*, 916.

30. Huang, J.; Xue, Y.; Sun, S.; Zhang, J. Spatial and temporal variability of drought during 1960–2012 in Inner Mongolia, north China. *Quat. Int.* **2015**, *355*, 134–144.

31. Cai, S.; Song, X.; Hu, R.; Leng, P.; Li, X.; Guo, D.; Zhang, Y.; Hao, Y.; Wang, Y. Spatiotemporal characteristics of agricultural droughts based on soil moisture data in Inner Mongolia from 1981 to 2019. *J. Hydrol.* **2021**, *603*, 127104.

32. Shen, Z.; Zhang, Q.; Singh, V.P.; Sun, P.; Song, C.; Yu, H. Agricultural drought monitoring across Inner Mongolia, China: Model development, spatiotemporal patterns and impacts. *J. Hydrol.* **2019**, *571*, 793–804.

33. Khan, N.Z.; Waseem, M. Assessment of Satellite Based Evapotranspiration Products at Regional Scale over Landscape of Pakistan. *Hydrology* **2022**, *10*, 34–41.

34. Wang, W.; Cui, W.; Wang, X.; Chen, X. Evaluation of GLDAS-1 and GLDAS-2 forcing data and Noah model simulations over China at the monthly scale. *J. Hydrometeorol.* **2016**, *17*, 2815–2833.

35. Sun, X.; Lai, P.; Wang, S.; Song, L.; Ma, M.; Han, X. Monitoring of extreme agricultural drought of the past 20 years in southwest China using GLDAS soil moisture. *Remote Sens.* **2022**, *14*, 1323.

36. Li, Y.; Huang, S.; Wang, H.; Zheng, X.; Huang, Q.; Deng, M.; Peng, J. High-resolution propagation time from meteorological to agricultural drought at multiple levels and spatiotemporal scales. *Agric. Water Manag.* **2022**, *262*, 107428.

37. Yang, M.; Yan, D.; Yu, Y.; Yang, Z. SPEI-based spatiotemporal analysis of drought in Haihe River Basin from 1961 to 2010. *Adv. Meteorol.* **2016**, *2016*, 7658015.

38. Abu Arra, A.; Şişman, E. Characteristics of Hydrological and Meteorological Drought Based on Intensity-Duration-Frequency (IDF) Curves. *Water* **2023**, *15*, 3142.

39. Ullah, I.; Ma, X.; Yin, J.; Omer, A.; Habtemicheal, B.A.; Saleem, F.; Iyakaremye, V.; Syed, S.; Arshad, M.; Liu, M. Spatiotemporal characteristics of meteorological drought variability and trends (1981–2020) over South Asia and the associated large-scale circulation patterns. *Clim. Dyn.* **2023**, *60*, 2261–2284.

40. Merabti, A.; Darouich, H.; Paredes, P.; Meddi, M.; Pereira, L.S. Assessing Spatial Variability and Trends of Droughts in Eastern Algeria Using SPI, RDI, PDSI, and MedPDSI—A Novel Drought Index Using the FAO56 Evapotranspiration Method. *Water* **2023**, *15*, 626.

41. Li, J.; Xi, M.; Pan, Z.; Liu, Z.; He, Z.; Qin, F. Response of NDVI and SIF to Meteorological Drought in the Yellow River Basin from 2001 to 2020. *Water* **2022**, *14*, 2978.

42. Wang, F.; Yang, H.; Wang, Z.; Zhang, Z.; Li, Z. Drought evaluation with CMORPH satellite precipitation data in the Yellow River Basin by using gridded standardized precipitation evapotranspiration index. *Remote Sens.* **2019**, *11*, 485.

43. Li, W.-y.; Wen, X.; Tan, Q.-f.; Tu, Y.-h.; Yang, T.-t.; Wang, Y.-l.; Yu, X.-d. Exploring spatio-temporal distribution and evolution of dry-wet alternation using a three-dimensional identification method. *J. Hydrol.* **2022**, *612*, 128119.

44. Sheffield, J.; Andreadis, K.M.; Wood, E.F.; Lettenmaier, D.P. Global and continental drought in the second half of the twentieth century: Severity–area–duration analysis and temporal variability of large-scale events. *J. Clim.* **2009**, *22*, 1962–1981.

45. Xu, K.; Yang, D.; Yang, H.; Li, Z.; Qin, Y.; Shen, Y. Spatio-temporal variation of drought in China during 1961–2012: A climatic perspective. *J. Hydrol.* **2015**, *526*, 253–264.

46. Liu, Y.; Zhu, Y.; Ren, L.; Singh, V.P.; Yong, B.; Jiang, S.; Yuan, F.; Yang, X. Understanding the spatiotemporal links between meteorological and hydrological droughts from a three-dimensional perspective. *J. Geophys. Res. Atmos.* **2019**, *124*, 3090–3109.

47. Wang, A.; Lettenmaier, D.P.; Sheffield, J. Soil moisture drought in China, 1950–2006. *J. Clim.* **2011**, *24*, 3257–3271.

48. Zhang, Z.; Lai, H.; Wang, F.; Feng, K.; Qi, Q.; Li, Y. Spatial–Temporal Patterns and Propagation Dynamics of Ecological Drought in the North China Plain. *Water* **2022**, *14*, 1542.

49. Su, L.; Miao, C.; Duan, Q.; Lei, X.; Li, H. Multiple-wavelet coherence of world's large rivers with meteorological factors and ocean signals. *J. Geophys. Res. Atmos.* **2019**, *124*, 4932–4954.

50. Poornima, S.; Pushpalatha, M.; Jana, R.B.; Patti, L.A. Rainfall Forecast and Drought Analysis for Recent and Forthcoming Years in India. *Water* **2023**, *15*, 592.

51. Miao, L.; Jiang, C.; Xue, B.; Liu, Q.; He, B.; Nath, R.; Cui, X. Vegetation dynamics and factor analysis in arid and semi-arid Inner Mongolia. *Environ. Earth Sci.* **2015**, *73*, 2343–2352.

52. Guo, W.; Huang, S.; Huang, Q.; She, D.; Shi, H.; Leng, G.; Li, J.; Cheng, L.; Gao, Y.; Peng, J. Precipitation and vegetation transpiration variations dominate the dynamics of agricultural drought characteristics in China. *Sci. Total Environ.* **2023**, *898*, 165480.

53. Wang, L.; Kotani, A.; Tanaka, T.; Ohta, T. Assessment of drought condition using remotely sensed drought severity index and its correlations with soil moisture product in Inner Mongolia. *Theor. Appl. Climatol.* **2020**, *141*, 715–728.

54. Na, Y.T. Overview of application of remote sensing on drought monitoring in Inner Mongolia. *Adv. Mater. Res.* **2014**, *955–959*, 3735–3739.

55. Zhao, H.; Chen, X.; Yang, J.; Yao, C.; Zhang, Q.; Mei, P. Comprehensive Assessment and Variation Characteristics of the Drought Intensity in North China Based on EID. *J. Appl. Meteorol. Climatol.* **2022**, *61*, 297–308.

56. Pan, Y.; Zhu, Y.; Lü, H.; Yagci, A.L.; Fu, X.; Liu, E.; Xu, H.; Ding, Z.; Liu, R. Accuracy of agricultural drought indices and analysis of agricultural drought characteristics in China between 2000 and 2019. *Agric. Water Manag.* **2023**, *283*, 108305.

57. Wang, Q.; Liu, Y.-y.; Zhang, Y.-z.; Tong, L.-j.; Li, X.; Li, J.-l.; Sun, Z. Assessment of spatial agglomeration of agricultural drought disaster in China from 1978 to 2016. *Sci. Rep.* **2019**, *9*, 14393.
58. Yang, P.; Zhai, X.; Huang, H.; Zhang, Y.; Zhu, Y.; Shi, X.; Zhou, L.; Fu, C. Association and driving factors of meteorological drought and agricultural drought in Ningxia, Northwest China. *Atmos. Res.* **2023**, *289*, 106753.